Ionics (2021) 27:2509–2525
https://doi.org/10.1007/s11581-021-04023-y

ORIGINAL PAPER

Dielectric relaxations and ion transport study of NaCMC:$NaNO_3$ solid polymer electrolyte films

Supriya K Shetty[1,2] · Ismayil[2] · Shreedatta Hegde[3] · V Ravindrachary[3] · Ganesh Sanjeev[3] · Rajashekhar F Bhajantri[4] · Saraswati P Masti[5]

Received: 1 February 2021 / Revised: 3 March 2021 / Accepted: 25 March 2021 / Published online: 13 April 2021

Abstract

Na^+ ion-conducting solid polymer electrolyte (SPE) of sodium salt of carboxymethyl cellulose (NaCMC) doped with sodium nitrate ($NaNO_3$) was developed by solution casting method. FTIR technique confirmed the formation of hydrogen bonding between NO_3^- anion and functional groups of NaCMC. XRD study revealed the low degree of crystallinity that reduced upon doping. Impedance spectroscopy was adapted in order to analyze the conductivity and dielectric relaxation phenomena of the polymer-salt complex. FTIR deconvolution technique was employed to understand the factor that influences the ionic conductivity in SPE; concentration of mobile ions and ionic mobility both play a vital role. Ion transference number has been found out to be > 0.97 for all samples indicating that the conducting species are primarily ions. The highest ionic conductivity of 3×10^{-3} Scm^{-1} with the mechanical strength of 30.12 MPa was achieved for a host containing 30 wt.% $NaNO_3$ at ambient temperature.

Keywords Solid polymer electrolytes · Sodium carboxymethyl cellulose · Sodium nitrate · Ionic conductivity · Transference number · Differential scanning calorimetry

Introduction

Rechargeable lithium-ion batteries (LIBs) are not only used to power the portable electronic gadgets and hybrid/electric vehicles but can also store a significant amount of energy from renewable resources making less reliant on fossil fuel, consequently leading to the substantial increase in the demand and supply for lithium. Since the co-relationship between supply and demand is a positive slope, the concentration of lithium in the Earth's crust plays a vital role. From 2010 onwards, research activity on sodium-ion batteries (SIBs), especially on electrolytes, has significantly amplified since the lithium concentration in the Earth's crust is less than 20 ppm, whereas sodium (27,500 ppm) is the fourth most abundant element and geographically well distributed on the Earth's crust [1, 2]. Even though Na^+ ions (1.02 Å) are bulky compared to Li^+ ions (0.76 Å) with higher standard electrode potential (− 2.71 V vs SHE) as compared to lithium (− 3.02 V vs SHE), which affects transport properties as well as the energy density of batteries [3], respectively, nevertheless, SIBs have certain advantages over LIBs such as lower expensive and less weight, because of the incorporation of aluminium as both positive and negative current collectors (as a contrast to lithium, sodium does not alloy with aluminium) [4]. From decades research is going on solid polymer electrolytes (SPEs) and has gained more attention in recent years due to its wide variety of application in devices such as sensors, fuel cell, supercapacitors, electrochromic window and analogy memory devices. Solvent-free solid polymer electrolyte (SPE) provides high safety and structural flexibility for cell fabrication compared with other counterparts with excellent thermal and chemical stability but exhibits moderate ionic conductivity at ambient temperature [5]. Ionic conductivity of SPEs for

✉ Ismayil
ismayil.mit@manipal.edu; ismayil.486@gmail.com

1 Department of Sciences, Manipal Academy of Higher Education, Manipal, Karnataka 576104, India

2 Department of Physics, Manipal Institute of Technology, Manipal Academy of Higher Education, Manipal, Karnataka 576104, India

3 Department of Physics, Mangalore University, Mangalagangotri, Karnataka 574199, India

4 Department of Studies in Physics, Karnataka University, Pavate Nagar, Dharwad, Karnataka 580003, India

5 Department of Chemistry, Karnataka University's Karnataka Science College, Dharwad, Karnataka 580001, India

electrochemical application is set to > 10^{-3} Scm^{-1} as a threshold value [4–6], and to attain it, there is a need for better understanding about the dissociation of a salt, interaction between the ions in the polymer matrix during transport mechanism, the coupling of the segmental relaxation with the ion transport, which is not completely well understood in polymer electrolyte [7], and therefore, sets the path for generating new energy storage systems. A choice of appropriate polymer and salt in the preparation of electrolyte is crucial since the polymer electrolyte properties depend on the molecular weight, glass transition temperature (T_g), the dielectric constant of the polymer as well as on the lattice energy of the salt [8]. The PE should be mechanically stable so that the systems could be scaled up and produced on a large scale, and in need, the SPE should withstand the stress generated during the charging and discharging of the battery [9], which depends on the structure and molecular weight of the polymer as well as on the polymer-salt complexation. Dielectric constant of the polymer plays a vital role in dissociating the salt and influencing the concentration of charge carriers in the SPE [10]. Ionic conductivity is not only sensitive to carrier concentration but also to the motion of ions and relaxation process that is strongly associated with T_g, above which segmental relaxation is observed. Thus, synthesis of novel low-cost solid polymer electrolyte exhibiting high ionic conductivity with suitable mechanical strength for new generation SIBs is still a challenge [11].

In the present scenario, it is vital to have a balance between energy need and environmental issues faced. Currently, to address current environmental issues towards a sustainable future, it is vital to use eco-materials, in all phases of product manufacturing. Biodegradable polymers/biopolymers are grabbing greater attention as polymer host for PEs other than medical, agricultural and goods packaging application, and this is because of their rich resource, non-toxicity, degradability, biocompatibility and excellent film-forming properties. Natural polysaccharides such as cellulose, starch, chitosan, pectin, alginate and carrageenan have emerged as the potential candidates as polymer host for solid biopolymer electrolytes and can be an excellent substitute for the synthetic polymer without compromising the properties needed for energy storage application. In the current work, sodium carboxymethyl cellulose (NaCMC) is of interest, due to its film-forming ability, material stability, non-toxic, biodegradable and biocompatibility [12, 13]. NaCMC, anionic polysaccharides, is produced by reacting cellulose with sodium monochloroacetate [14]. NaCMC has emerged as a promising green alternative electrolyte material compared to environmentally unfriendly polymers [15, 16], leading to enhancement in battery properties. The functional groups present in the backbone of NaCMC not only facilitate the salt dissociation but also trap anions by forming a hydrogen bond between them. It helps in the enhancement of ionic conductivity of the polymer electrolyte. It is evident from the literature survey that Li^+, H^+ conducting polymer electrolytes based on NaCMC have been reported, e.g. Gupta et al. [17] recently reported NaCMC: $LiBF_4$ system with ionic conductivity 8.2 × 10^{-6} Scm^{-1}. Ahamad et al. [18] reported conductivity of 1.43 × 10^{-3} Scm^{-1} for unplasticized polymer electrolyte of NaCMC-NH_4Cl. Samsudin et al. [19] reported room temperature conductivity of 1.12 × 10^{-4} Scm^{-1} for NaCMC: NH_4Br system. Chai et al. [20] got an ionic conductivity of 2.11 × 10^{-5} Scm^{-1} for proton-conducting NaCMC doped with oleic acid. As per the literature survey to date, no one had doped NaCMC with $NaNO_3$, and the present work is focused on Na-ion-conducting solid polymer electrolyte. The present work is focused on developing solid polymer electrolyte film with appreciable ionic conductivity as well as suitable mechanical strength for energy storage application.

Experimental section

Materials

Sodium carboxymethyl cellulose (NaCMC, average molecular weight 198,447 g/mol and viscosity 1100–1900 cPs) was purchased from s. d. fine-Chem. Pvt. Ltd., Mumbai, India, and sodium nitrate ($NaNO_3$) was procured from Merck Life Science Private Limited, Bengaluru, India.

Synthesis of polymer electrolytes

Solid bio-polymer electrolyte film based on NaCMC doped with various percentage of sodium nitrate salt was prepared by the traditional solution casting method, double distilled water being the common solvent. The different weight percentage of sodium nitrate salt varying from 5, 10, 15, 20, 25 and 30 (designated as CN5, CN10, CN15, CN20, CN25 and CN30) were added into NaCMC solution and stirred continuously for 5 h at 50 °C until a clear homogenous solution was obtained. Once the viscous solution was obtained, the mixture was poured into clean glass Petri dishes and allowed for drying at room temperature. Polymer electrolyte films (around 200-micron thickness) were peeled off from the Petri dish and were kept in hot air oven at 45 °C for 24 h to ensure the elimination of the traces of solvent. The films were stored in a desiccator for further characterization.

Characterization techniques

IRPrestige-21 FTIR SHIMADZU was utilized to obtain FTIR spectra in the transmittance mode in the wavenumber range 4000–400 cm^{-1} with the resolution of 4 cm^{-1} where the spectroscopy has been equipped with attenuated total reflection (ATR) accessory with the diamond crystal. X-ray diffraction pattern was

recorded by 3rd generation Empyrean, Malvern Panalytical diffractometer with X-ray source: Cu-K_α radiation of wavelength (1.5406 Å) in the range 10°–60°. DSC measurements were carried out on SHIMADZU DSC-60 PLUS MODEL taken at a heating scan rate of 10 °C/min under nitrogen atmosphere in the temperature range 30–250 °C. Agilent 4294A precision impedance analyzer in the frequency range of 40 Hz to 5 MHz was adopted to carry out electrical studies at ambient temperature. The sample was cut into an appropriate size and placed between silver blocking electrodes of the contact area 0.25 cm^2 with a voltage signal of 500 mV. Inbuilt software was used to measure the real (Z'), imaginary (Z'') impedance, parallel capacitance (C_p) and loss factor (tan δ) at various frequencies. I-V characteristics (electrochemical potential window) and transference number measurements were carried out using KEITHLEY 2636B source metre with the help of a spring-loaded system with stainless steel being the blocking electrode (SS/SPE/SS). Mechanical properties at room temperature were carried out using a universal testing machine (UTM), Dak System Inc. 7200 series, at a crosshead speed of 0.1 mm/min where the polymer/polymer electrolytes in a rectangular shape of gauge length 50 mm and width of 25 mm were used, according to ASTM D882 standards.

Results and discussions

FTIR spectroscopy

FTIR is the tool to visualize the polymer structure and the interaction/complexation between polymer host and the salt, observed from the change brought about in the IR spectra. The interaction taking place between the polymer and metal ions depends on the factors such as the type of the functional groups attached to polymer main chain, type and charge of ions [21]. FTIR spectra of pure NaCMC, $NaNO_3$ and polymer complexes were recorded in the transmittance mode, as shown in Fig. 1a, and possible vibration mode and wavenumber are tabulated in Table 1. A strong and broad absorption band appearing in the 3700–3000 cm^{-1} region indicates plenty of hydroxyl (–OH) group attached to the main chain of the polymer [22, 23]. The band at 2924 cm^{-1} is due to –CH stretching vibration [24]. The sharp and strong absorption band at 1584 cm^{-1} is assigned to the carboxylate anion group (COO^-) [25], and the remaining bands at 1409 cm^{-1}, 1327 cm^{-1} and 1053 cm^{-1} ascribed to $–CH_2$ scissoring, –OH bending and C–O–C stretching [22, 24, 26], respectively, and are considered to be the signature peaks of NaCMC. FTIR spectra of $NaNO_3$ exhibits three prominent peaks at 3448 cm^{-1} (presence of –OH group, i.e., moisture content) [27], and the intense peak at 1340 cm^{-1} corresponds to asymmetric stretching mode, $\gamma_3\left(NO_3^-\right)$ of nitrate anion and a peak at 832 cm^{-1}, corresponding to out of plane deformation mode $\gamma_2\left(NO_3^-\right)$ of the free NO_3^- [28, 29]. An observable change in vibration mode, peak intensity or change in the shape of the absorption band indicates the occurrence of complexation between the ions and the polymer [30, 31]. Correspondingly, a noticeable change in the shape of the band corresponding to $–CH_2$ scissoring and –OH bending has been observed compared to other bands, where the spectra exhibited broadness in peak corresponding to $–CH_2$ scissoring with an increase in salt content as depicted in Fig. 1b. A decrease in peak intensity/disappearance

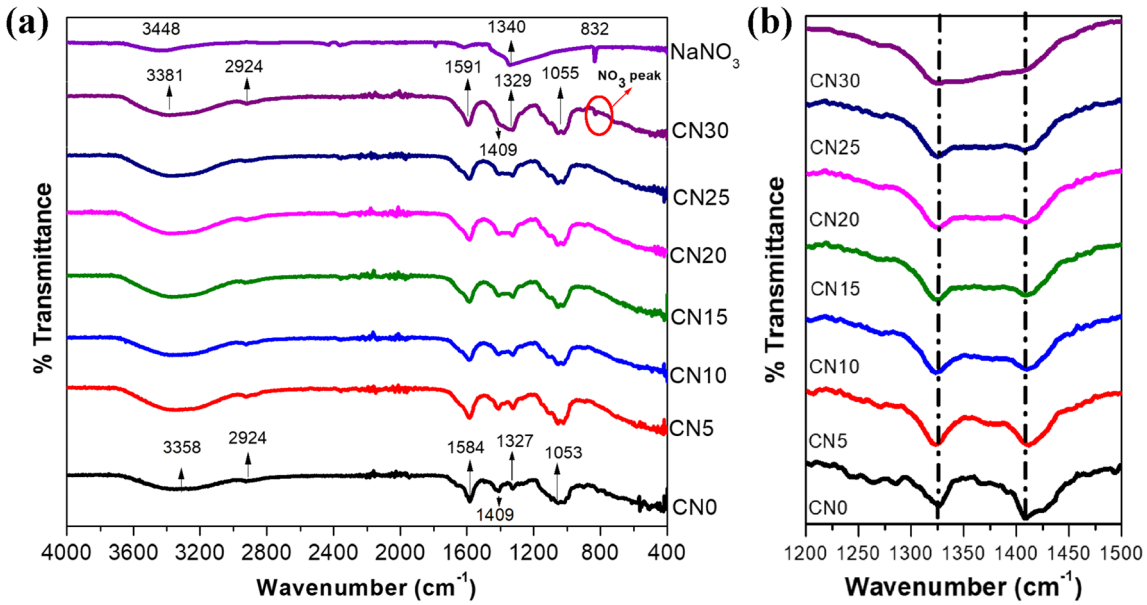

Fig. 1 **a** FTIR spectra of NaCMC, $NaNO_3$, and $NaNO_3$ doped NaCMC polymer electrolyte films. **b** FTIR spectra of NaCMC-$NaNO_3$ SPE in the region 1200–1500 cm^{-1}

Table 1 FTIR band assignment of NaCMC:$NaNO_3$ solid polymer electrolyte

NaCMC:$NaNO_3$ (Wavenumber cm^{-1})							Band assignment
CN0	CN5	CN10	CN15	CN20	CN25	CN30	
3358	3314	3381	3368	3387	3364	3381	–OH stretching
2924	2924	2928	2932	2922	2930	2924	–CH stretching
1584	1584	1584	1584	1584	1585	1591	COO^- asymmetric stretching of carboxylate anion
1409	1412	1410	1410	1410	1406	1409	$–CH_2$ scissoring
1327	1323	1323	1323	1325	1325	1329	–OH bending
1053	1055	1053	1053	1055	1055	1055	C–O–C stretching

of the peak upon doping is due to solvation of anion via hydrogen bonding between the hydroxyl functional group of the polymer and the oxygen of the anion. The shift in the frequency is correlated to force constant and bond length. The force constant values can be calculated [32] using the relation,

$$\overline{\vartheta} = \frac{1}{2\pi c}\sqrt{\frac{k(m_1+m_2)}{m_1 m_2}} \quad (1)$$

where $\overline{\vartheta}\,(cm^{-1})$ is the wavenumber, c is the velocity of light (3×10^{10} cms^{-1}), k is the force constant (Ncm^{-1}), m_1 and m_2 are atomic weights of two atoms, respectively. The force constant values for –OH and –CH bands for NaCMC and NaCMC:$NaNO_3$ has been evaluated and tabulated in Table 2. The force constant change for –OH and –CH upon doping indicates interaction of NO_3^- anion with the hydrogen of the –OH and –CH functional group. Figure 2a and b schematically represents NaCMC and its interaction with nitrate anion after doping respectively.

XRD analysis

Solid polymer electrolyte structure and variation of its crystallinity were investigated through XRD analysis. Figure 3 depicts the XRD spectra of $NaNO_3$ salt, pristine and doped NaCMC. XRD spectra of $NaNO_3$ exhibits sharp peaks that indicate its crystalline nature, and the peaks are absent in the pattern of the complex system, demonstrating the complete dissolution of the salt in the polymer matrix. NaCMC exhibited two peaks at 2θ = 13°, 21° corresponding to the crystalline plane (110) and (200), respectively [33], associated with the low crystallinity of its structure. Broadening of the peak in region 20°–25° upon addition of the salt indicates the enhancement of amorphous phase, and thus XRD diffractograms were deconvoluted using Gaussian function using software Fityk 1.3.1 [34], in order to evaluate the degree of crystallinity using the following Eq. 2 [35], and are tabulated in Table 3 and shown in Fig 4.

$$X_c = \frac{A_c}{A_{c+}A_a} \times 100\% \quad (2)$$

where A_c is an area of the crystalline region, A_a is an area of the amorphous region and $X_c$is the percentage of crystallinity. Emerging of the new amorphous peak at the shoulder for a higher concentration of salt in the matrix in the deconvoluted spectra illustrates the increase in amorphous nature; SPE containing 30 wt% of $NaNO_3$ is in a more amorphous state. X-ray diffraction studies confirmed the fact that there exists definite complex coordination between NaCMC and $NaNO_3$.

Table 2 FTIR modes of –OH and –CH band variations in NaCMC:$NaNO_3$ SPE films

Samples	–OH band vibration		–CH band variation	
	Wavenumber (cm^{-1})	Force constant (Ncm^{-1})	Wavenumber (cm^{-1})	Force constant (Ncm^{-1})
CN0	1327	9.85	1409	10.89
CN5	1323	9.79	1412	10.94
CN10	1323	9.79	1410	10.91
CN15	1323	9.79	1410	10.91
CN20	1325	9.82	1410	10.91
CN25	1325	9.82	1406	10.85
CN30	1329	9.88	1409	10.89

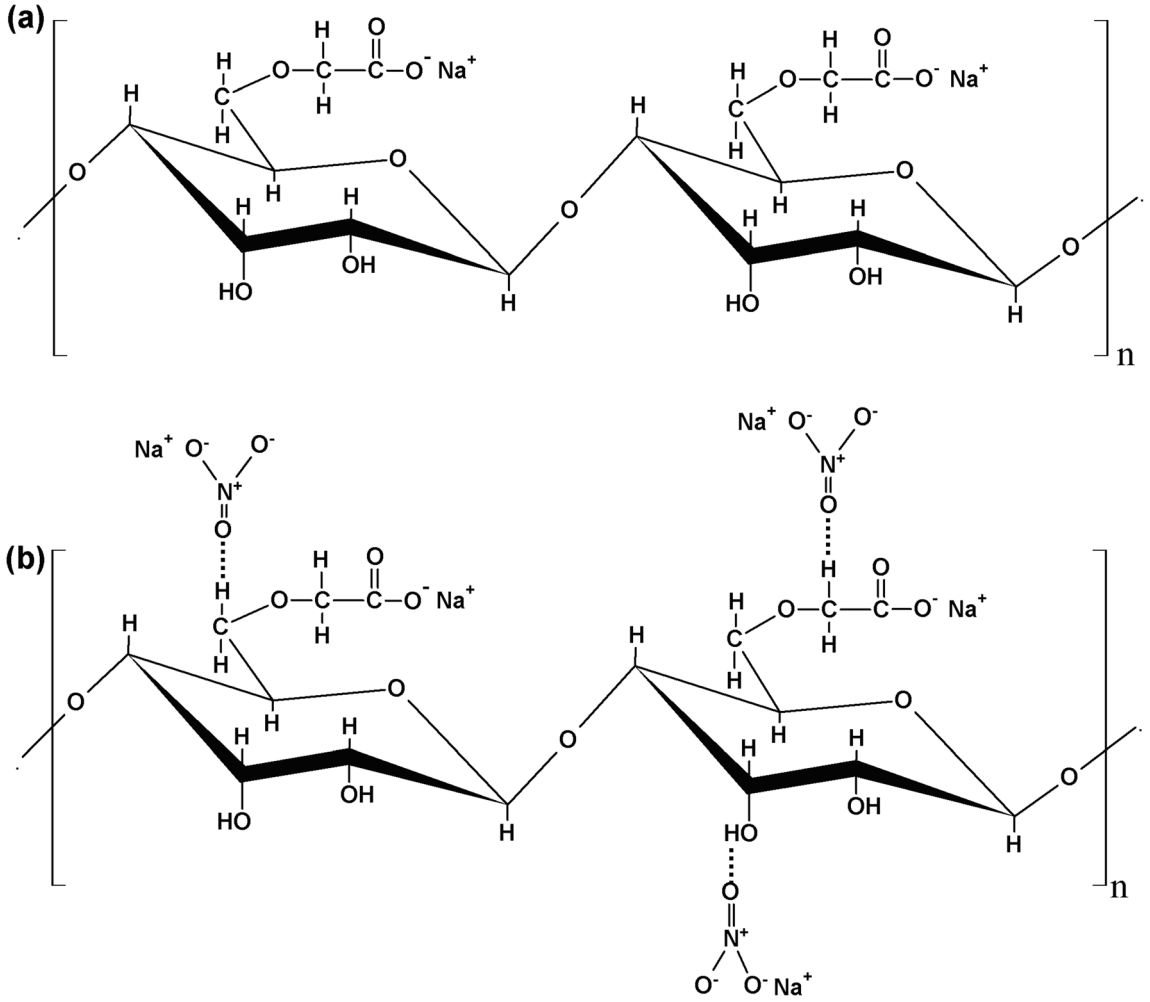

Fig. 2 **a** Chemical structure of NaCMC. **b** probable interaction between anion and hydroxy functional group of NaCMC

Thermal analysis

DSC measurement has been employed to monitor the impact of $NaNO_3$ on the transition of polymer chains of NaCMC. Figure 5 exhibits the DSC thermograms for pure polymer and its complexes in the temperature range of 30–250 °C. DSC curve exhibits a shallow and broad endothermic peak around the temperature range of 30–110 °C, due to water evaporation. A step-like transition rather than a peak is observed in the thermograms (characteristics of polysaccharides), and it corresponds to T_g of the polymer/polymer electrolyte [36]. A significant increase in T_g with an increase in salt concentration, attributed to the stiffening of the polymer chains due to intermolecular interaction between the NO_3^- anion with the functional group in the polymer chain,

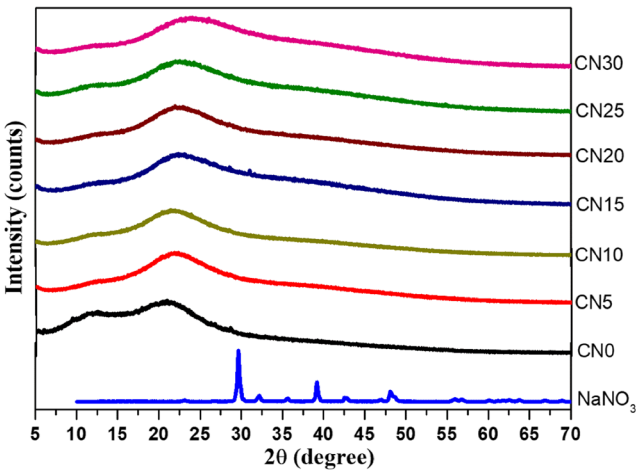

Fig. 3 XRD pattern of (NaCMC:$NaNO_3$) SPE system

Table 3 Percentage crystallinity of SPEs

Sample	A_C	A_a	Crystallinity (X_c) %
CN0	5553.48	38534.5	17.63
CN5	9264.65	76978.1	10.74
CN10	9966.33	83820.1	10.63
CN15	7712.55	72039.3	9.67
CN20	7477.16	80686.7	8.48
CN25	5829.34	70803.8	7.61
CN30	4660.41	75233.5	5.83

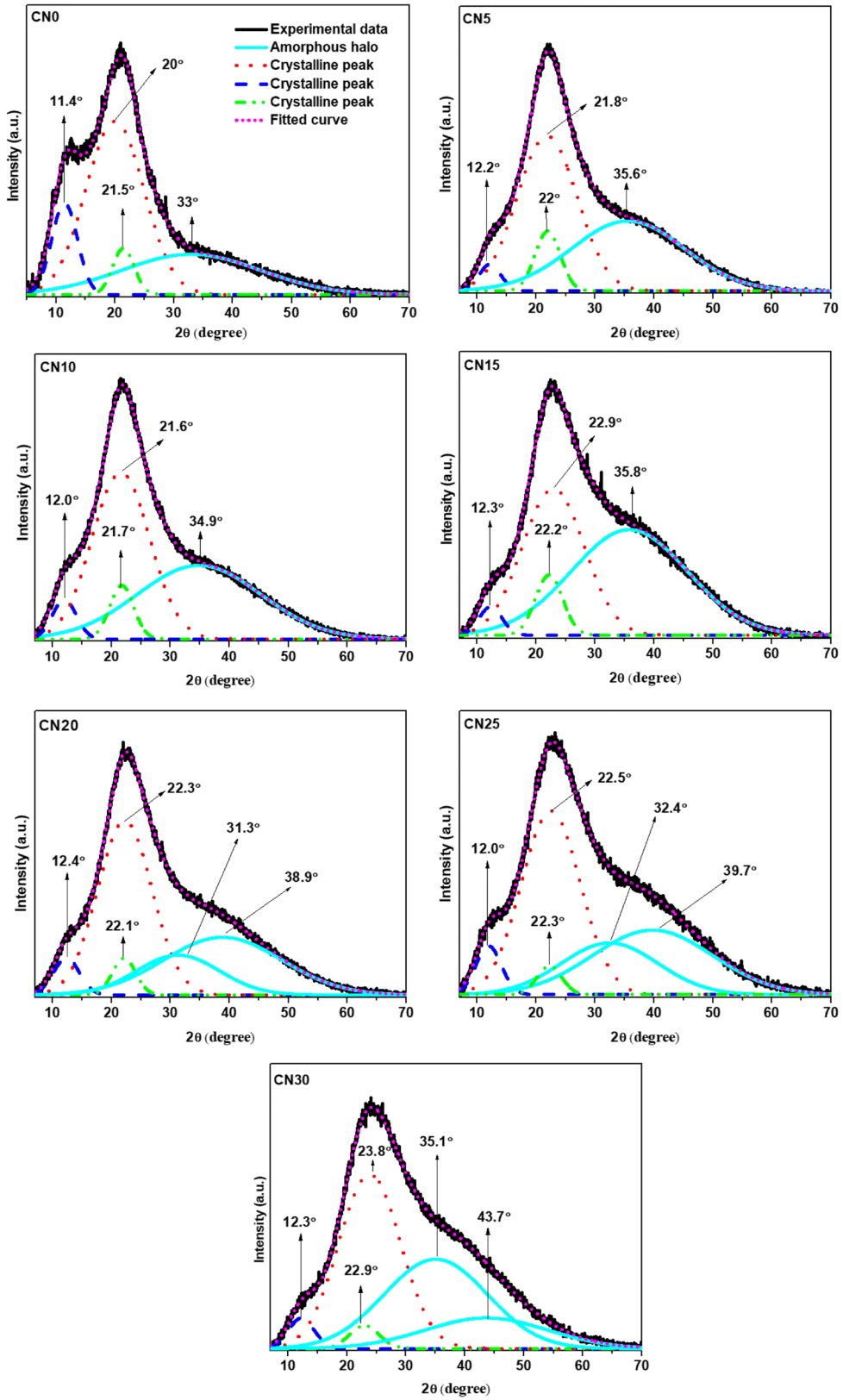

Fig. 4 XRD deconvolution of SPE for various compositions

and the interaction is via hydrogen bonding between the oxygen of NO_3^- with the hydrogen of –OH and $–CH_2$ groups (as schematically represented in Fig. 2) that has caused hindering of polymer chain flexibility. CN20, CN25 and CN30 exhibit

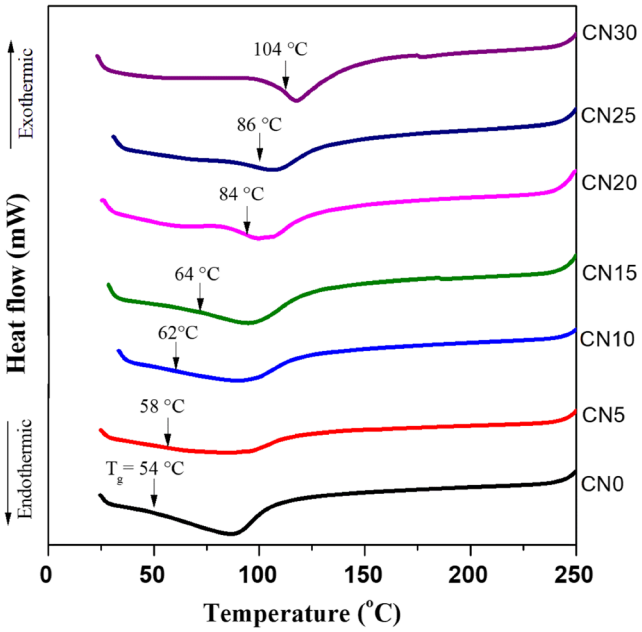

Fig. 5 DSC thermograms of undoped and doped NaCMC polymer

high T_g – transition implying the complexity in chain dynamics owing to network heterogeneity [37] that may be caused due to the formation of transient crosslinks between the polymer chains either by Na^+ ion or $Na^+\cdots NO_3^-\cdots Na^+$ bridges with the carboxylate group (C=O), and its probability is high at a higher salt concentration due to the availability of many free ions.

Impedance spectroscopy

Impedance spectroscopy was adopted to investigating the ion dynamics and relaxation processes that are taking place in the polymer electrolyte. Equations 3 and 4 [38] were used to fit the Cole-Cole plot, until the fitted point quite accurately matched with plot obtained from the impedance measurement. Parameters k_1, k_2, p_1, p_2 and R that were obtained from EIS spectrum analyzer software with average error percentage being less than 5% were employed for fitting.

$$Z' = \frac{R + R^2 k_1^{-1}\omega^{p_1}\cos\left(\frac{\pi p_1}{2}\right)}{1 + 2Rk_1^{-1}\omega^{p_1}cos\left(\frac{\pi p_1}{2}\right) + R^2 k_1^{-2}\omega^{2p_1}} + \frac{\cos\left(\frac{\pi p_2}{2}\right)}{k_2^{-1}\omega^{p_2}} \quad (3)$$

$$Z'' = \frac{R^2 k_1^{-1}\omega^{p_1}\sin\left(\frac{\pi p_1}{2}\right)}{1 + 2Rk_1^{-1}\omega^{p_1}\cos\left(\frac{\pi p_1}{2}\right) + R^2 k_1^{-2}\omega^{2p_1}} + \frac{\sin\left(\frac{\pi p_2}{2}\right)}{k_2^{-1}\omega^{p_2}} \quad (4)$$

where R, bulk resistance; k_1^{-1}, geometrical bulk capacitance; k_2^{-1}, the capacitance of the electric double layer formed at the electrolyte/electrolyte interface; p_1, the ratio of the angle between the diameter of the semicircle and Z''- axis; and p_2, a skew parameter that controls the degree of the tendency of the tilted spike from the Z'−axis. The impedance plot (Z' *vs* Z'') for different compositions that are depicted in Fig. 6 comprises two well-defined regions, slanted spike and depressed semicircle at low and high frequencies, respectively. A semicircle corresponds to the bulk response of the electrolyte, and a tilted spike corresponds to the accumulation of ions at the electrode/electrolyte interface. Each process can be well separated and can be represented by an electrical component. An equivalent circuit (model) obtained while fitting can be used to describe the impedance plot, where a semicircle is represented by the parallel combination of bulk resistance (R_b) and bulk capacitance (C_b), suggesting a parallel process of ion-conduction and dipolar/orientational polarization that is happening at high frequency [39, 40], and, spike, represented by the double-layer capacitance (C_{dl}), whose magnitude can be estimated from the relation, $Z'' = 1/2\pi f C_{dl}$, where C_{dl} is the capacitance at the frequency f. The plot is deviating from the ideal case, were, at low frequency, Z-plot must have exhibited a parallel line to the Z''- axis and semicircular arc with centre on the Z'- axis at the high-frequency end, and therefore, C_b and C_{dl} symbolised by constant phase element CPE2 and CPE1, respectively. A CPE has the property of R and C, the double-layer capacitance (C_{dl}), is replaced by CPE1 (a parallel combination of C_{dl} with R_{int}) and includes the double layer capacitance and interfacial resistance [41]. The capacitance of the electric double layer (k_2^{-1}) obtained using non-linear least square software (EIS spectrum analyzer) has been tabulated in Table 4 and found to increase with salt concentration indicating the availability of free ions at the electrode/electrolyte interface. The orientational polarization is represented by a constant phase element (CPE2) since the polar functional group attached in the polymer chain gets polarized in the AC field and hence can be represented by a capacitor [42]. Deviation of the plot on the complex impedance plane may be due to unevenness or roughness of the electrode/electrolyte interface due to imperfectness in the electrode and electrolyte surfaces [43]. The bulk ionic conductivity estimated from the complex-impedance plot using the relation $\sigma = t/R_b A$, where t, A and R_b is the thickness, area of the electrode and bulk resistance of the specimen, respectively, is tabulated in Table 4. Bulk resistance of the film found to decrease with an increase in salt concentration, either due to an increase in charge carrier concentration or due to enhancement in the amorphous region as depicted in the XRD pattern, leading to smooth migration of ions.

AC conductivity study

The analysis of frequency-dependent conductivity was conducted in order to understand the ion dynamics in the polymer electrolyte. The complex conductivity is

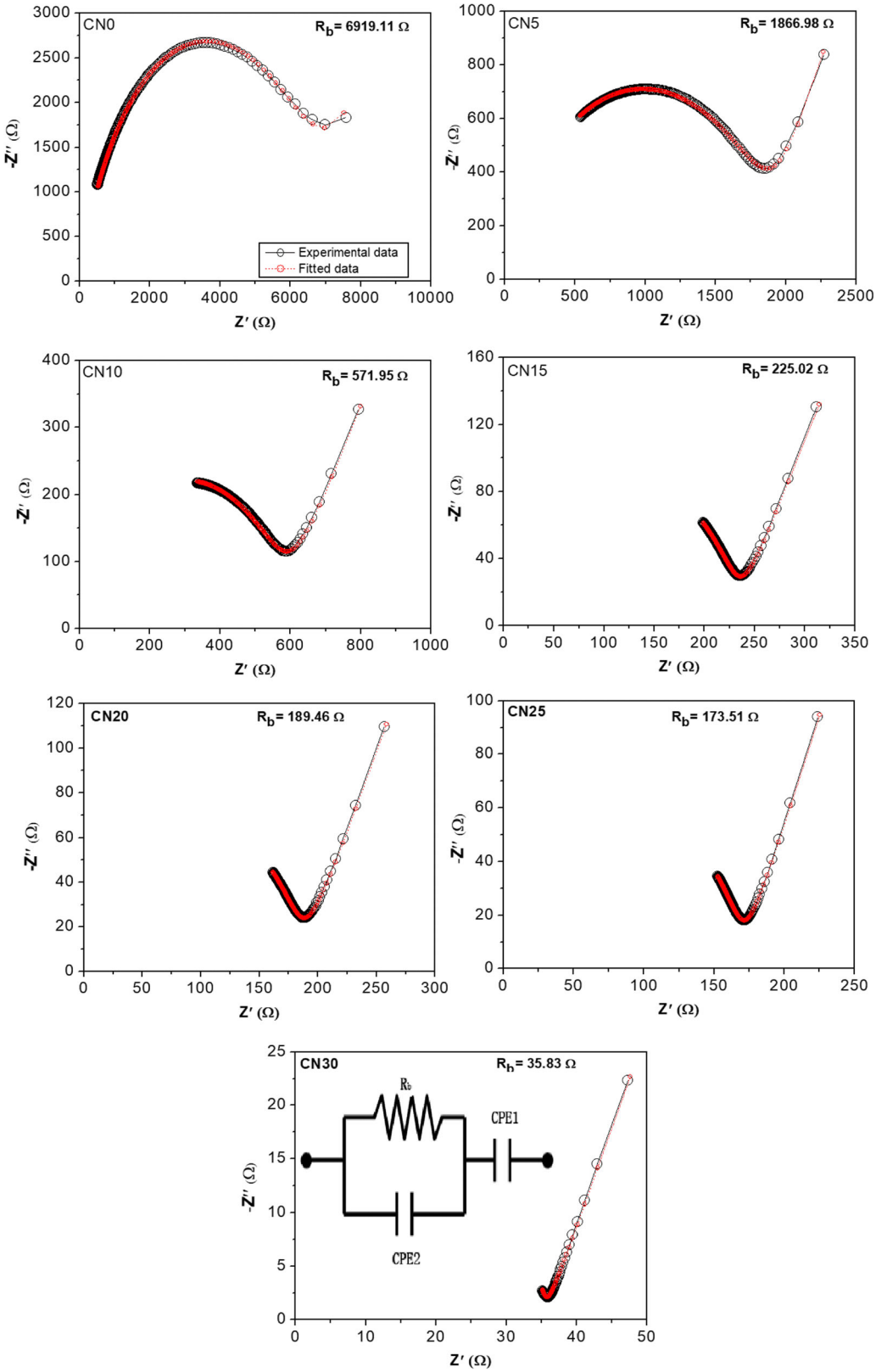

Fig. 6 Illustrates the Cole-Cole plot of the polymer electrolyte system for different weight percentage of sodium nitrate salt in NaCMC host

expressed as $\sigma^*(\omega) = \sigma'(\omega) + i\sigma''(\omega)$, real part of ac conductivity of the polymer electrolyte was obtained from the dielectric loss (ε'') using the relation [44], $\sigma' = \sigma_{ac} = \omega\varepsilon_o\varepsilon'' = \omega\varepsilon_o\varepsilon' \tan\delta$, where ε_o, dielectric

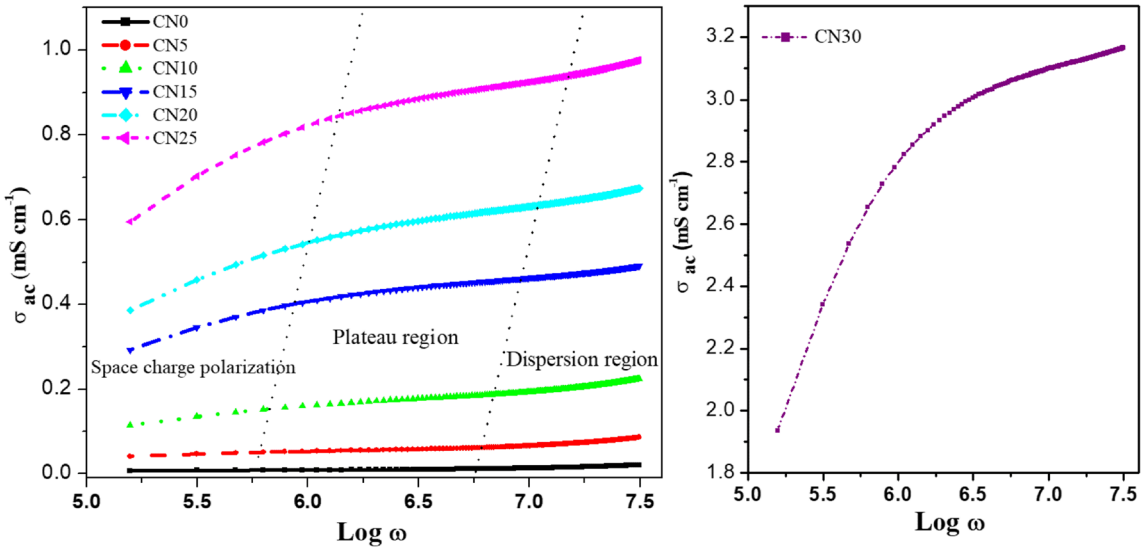

Fig. 7 Frequency-dependent conductivity spectra of the electrolyte films

permittivity in free space, tanδ, loss factor, $\omega = 2\pi f$, f being the frequency of the signal. Figure 7 shows the frequency dependence conductivity for various concentrations of salt in the host, and spectra compromise of three diverse regions associated with different phenomena: (i) low-frequency dispersive region, describing electrode-electrolyte interfacial phenomenon identified as *space charge polarization/electrode polarization*. At low frequencies, ions have enough time to accumulate at the electrode/sample interface resulting in the formation of electrical double layer capacitance (C_{dl}), under the influence of the field, leading to low ionic conductivity value at low frequency, since no mobile ions are available in the bulk of the sample [5, 45, 46]. (ii) Plateau region, due to ion conduction, resulting dc conductivity (σ_{dc}) is obtained by extrapolating the plateau region (at $\omega \rightarrow 0$) to σ_{ac} axis. (iii) A high-frequency power-law region where further increase in conductivity is observed, regions ii and iii can be explained by jump relaxation model, according to which cations jump from one coordinate site to another vacant neighbouring site in the polymer matrix and thus contributing to conductivity and high-frequency conductivity dispersion are observed due to probability of the correlated forwards-backwards hopping of ions along with the relaxation of the dynamic cage potential; thus the curve obtained found to obey the Jonscher universal power-law given by, $\sigma_{ac}(\omega) = \sigma_{dc} + A\omega^{s}$, where A and s are material parameters and s varies between 0 and 1 and A depends on the temperature of the composition [47, 48]. A general trend of σ_{ac} as the function of frequency has been observed for different samples that are observed in ion-conducting glass and plateau region shifted to higher frequency end with the increase in salt concentration. A switch from the frequency-independent to the frequency-dependent region is the beginning of conduction relaxation process [49]. Ion conduction in the PE may take place owing to two distinct events, first due to ion conduction via hopping and second by the segmental motion of polymer chain that facilitates coduction, either by providing the pathway for ions to move or by facilitating ions to hope from one site to others [50]. The former one is observed in crystalline/semicrystalline/amorphous polymer electrolytes, and for later one to happen, free volume plays a vital role that is affected by the amorphosity of the sample. Enhancement in conductivity with increase in salt concentration can be related to the enhancement in ion concentration in the polymer matrix and not due to enhancement in segmental motion of polymer chain; since T_g is above room temperature as observed from DSC curve. The highest ionic conductivity of 3×10^{-3} Scm^{-1} was obtained for 30 wt% of $NaNO_3$ in polymer matrix due to enhancement in amorphous phase. Bulk conductivity obtained from the Cole-Cole plot and the DC conductivity derived from the spectra of AC conductivity as tabulated in Table 4 shows a good agreement with each other.

Table 4 Bulk resistance (R_b), bulk conductivity, DC conductivity (σ_{dc}) and relaxation

time for pristine and doped NaCMC

Sample	Bulk resistance (R_b) (Ω)	Bulk conductivity (Scm^{-1})	DC conductivity (σ_{dc}) at ω = 0 (Scm^{-1})	Relaxation time τ (s)	$k2-1k_2^{-1}$ (10^{-6} F)
CN0	6919.11	8.32×10^{-6}	10.4×10^{-5}	-	-
CN5	1866.98	5.59×10^{-5}	6.84×10^{-5}	9.09×10^{-7}	0.32
CN10	571.95	1.86×10^{-4}	1.88×10^{-4}	4.90×10^{-7}	1.88
CN15	225.02	4.76×10^{-4}	4.61×10^{-4}	2.36×10^{-7}	3.22
CN20	189.46	6.18×10^{-4}	6.20×10^{-4}	2.27×10^{-7}	4.69
CN25	173.51	9.03×10^{-4}	9.11×10^{-4}	2.20×10^{-7}	3.62
CN30	35.83	3.12×10^{-3}	3.08×10^{-3}	7.86×10^{-8}	10.78

Dielectric study

Structural relaxation and ion dynamics in PEs can be explored from the dielectric measurements, where the SPE is sandwiched between the electrodes and exposed to the alternating field. Numerous types of polarization can happen depending on the material such as electronic, atomic, dipolar and space charge polarization/interfacial polarization. Each polarization is characterized by its own relaxation time, which vary from one material to others. In the given frequency window of the study, interfacial polarization and orientational polarization are effective, since electronic and atomic polarization takes place at higher frequencies and is instantaneous in a dielectric study of the polymer [51, 52]. Dielectric parameters are associated with the relaxation process compromising structural relaxation and conductivity relaxation. Structural relaxation is either related to the rotational orientation of the dipole attached to the polymer main chain known as dipolar relaxation or segmental relaxation process (requires the presence of free volume). The complex permittivity has been employed to describes dipole relaxation phenomena in polymer electrolyte system, defined as $\varepsilon^*(\omega) = \varepsilon'(\omega) - j\varepsilon''(\omega)$, the real part talks about the ability of the polymer to dissociate the ions, which depends on the functional group attached to the polymer. It is also the measure of electric potential energy stored in the material under the action of the field due to induced polarization [53], and complex part, known as dielectric loss,ε'', accounts for the energy required to align dipoles

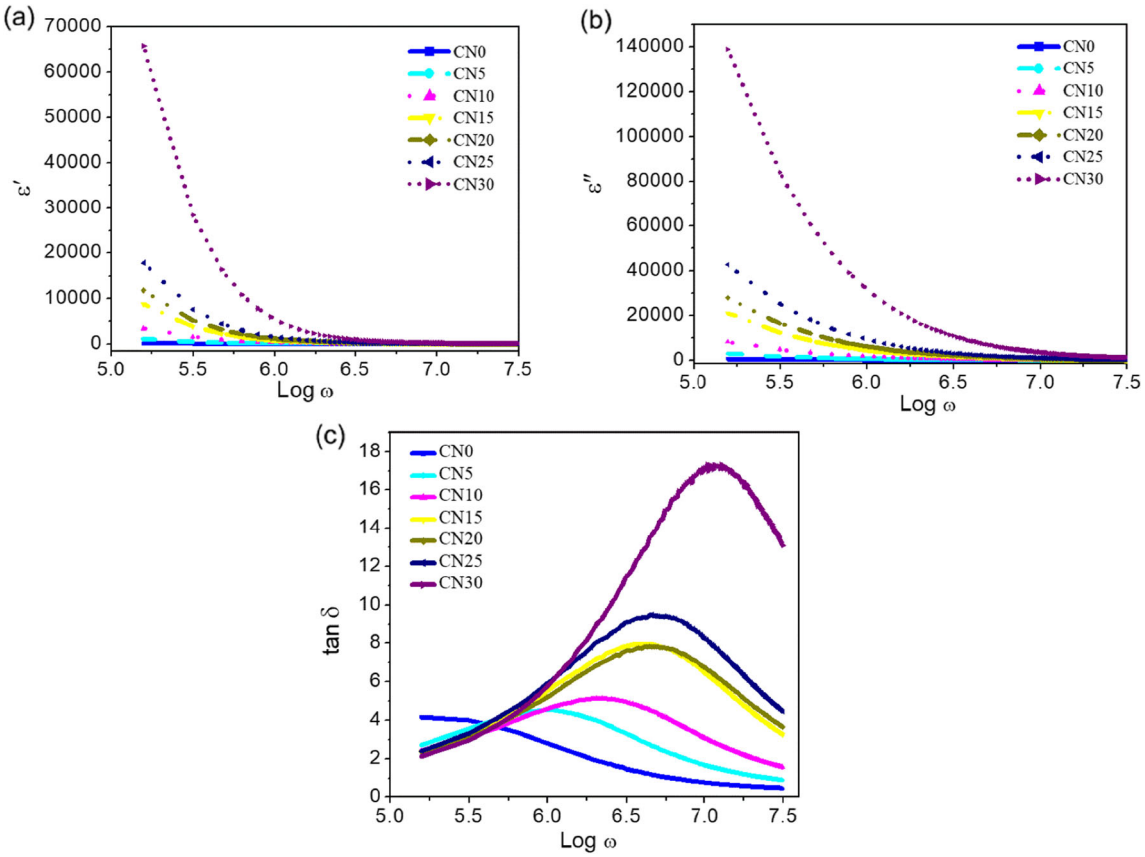

Fig. 8 Frequency dependence of **a** ε', (**b**) ε'' and (**c**) tan δ for different salt concentrations in NaCMC polymer

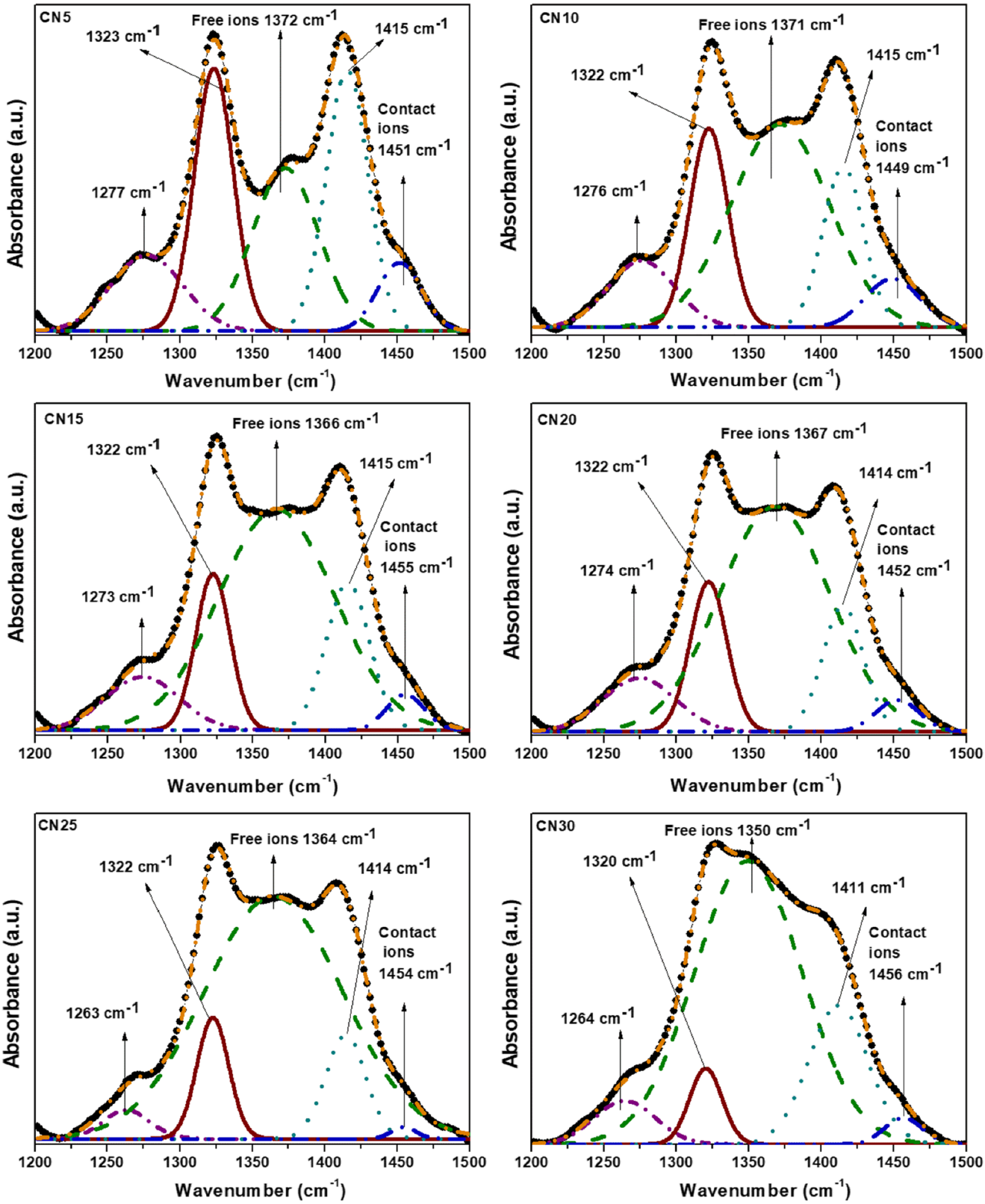

Fig. 9 FTIR deconvolution of NaCMC with different weight percentages of salt in 1200–1500 cm^{-1} region

and move ions in the field. The real and imaginary part of complex permittivity were evaluated using the relation $\varepsilon' = C_p t/\varepsilon_o A$, $\varepsilon'' = \varepsilon' \tan\delta$, where t, the thickness of the film; A, electrode area; C_p, geometrical capacitance; and $tan\delta$, loss

Table 5 Values of the free ions (%), η, μ and D obtained using the FTIR deconvolution method

Sample	Area of free ions (A_f)	Area of contact ions (A_c)	Free ions (%)	No. of mobile ion, η ($\times 10^{20}$ cm^{-3})	Ionic mobility, μ ($\times 10^{-6}$ cm^2 V^{-1} s)	Diffusion coefficient, D ($\times 10^{-8}$ cm^2 s^{-1})
CN5	4.22	1.18	78.15	4.13	0.85	2.21
CN10	8.90	1.18	88.29	9.51	1.22	3.19
CN15	12.71	0.66	95.06	15.65	1.90	4.97
CN20	14.68	0.81	94.77	21.19	1.82	4.76
CN25	17.51	0.14	99.21	28.26	2.00	5.22
CN30	27.84	0.9	96.87	33.76	5.78	15.09

factor. Figure 8a and b exhibits larger value of ε' & ε'' at a low frequency region related to the interfacial polarization, which could be associated with the increase of charge carrier concentration at the interface and not related to the bulk property of the dielectric that is commonly observed in SPEs. At very low frequency, ions have sufficient time to build up at the interface giving rise to a large value and thereafter decreases nonlinearly with frequency and approaches steady state known as limiting permittivity ε_∞ , nearly at 3MHz, due to inefficiency of the system to follow fast reversal of the field. No relaxation peaks are observed in the plot of ε'' Vs log ω, indicating that the enhancement in the conductivity is due to the increase in the density of the ions and not because of the structural relaxation process [54]. ε'' is high at low frequency due to free charge motions within the material [55]. It is observed that ε' and ε'' increase with salt content, attributed to an increase in charge carrier concentration. ε' shows increases with increase in dopant concentration showing the correlation between the dielectric constant and charge carrier density, as expressed by the equation [56, 57], $n = n_o \exp\left[-\frac{U}{kT\varepsilon}\right]$, where n is charge carrier concentration, U is the salt dissociation energy and ε is dielectric constant. n depends on the dissociation energy of the salt. Generally, for any medium, conductivity is given by $\sigma = \sum_i n_i\, q_i\, \mu_i$ and holds for PE system too, where i stands for conductivity due to different types of conducting species and q and μ stand for charge and mobility of conducting ions. Increase in conductivity in PEs may be due to (i) increase in charge carrier concentration, (ii) increase in amorphousness and (iii) segmental relaxation of the polymer. Figure 8c shows the variation of loss factor (tan δ) as the function of frequency displays maximum at characteristics frequency, which suggests the presence of conductivity relaxation, the relaxation time (τ) evaluated using the equation $\omega_{max}\tau = 1$, where ω_{max} corresponds to the maximum of (tan δ) peak. The relaxation peak of the pristine is at a lower frequency range and hence is not observed in the plot. The relaxation peaks got shifted to higher frequency end with an increase in salt concentration leading to a decrease in relaxation time indication improvement in ion dynamics and hopping rate [58]. A decrease in relaxation time with increase in salt concentration has been observed in the matrix and may be attributed to the increase in the mobility of the ions in the polymer complex [59], due to enhancement in the amorphous phase as justified by XRD [60].

Transport property study

Fundamental properties (η, μ and D) of NaCMC:$NaNO_3$ SPE system has been evaluated by FTIR deconvolution. Deconvolution technique was performed using Origin Lab Pro 9 software. Prior to deconvolution, the spectrum of the SPEs was converted into absorbance mode, and then baseline correction were carried out followed by multiple peak fit using Gaussian function. FTIR deconvolution is done in the region between 1200 and 1500 cm^{-1}, due to the presence of the asymmetric stretching of anion NO_3^- at 1340 cm^{-1} and the change it brought about in the region corresponding to –OH bending and CH_2 scissoring as depicted in Fig. 9. Deconvoluted region comprises five bands, band at ~ 1278–1262 cm^{-1} corresponds to C-C (skeleton vibrations) [61]. A peak at ~ 1322 cm^{-1} and 1414 cm^{-1} corresponds to characteristics peak of NaCMC due to –OH bending and CH_2 scissoring, respectively. The band observed in the wavenumber region 1375–1348 cm^{-1} was assigned to free ions,

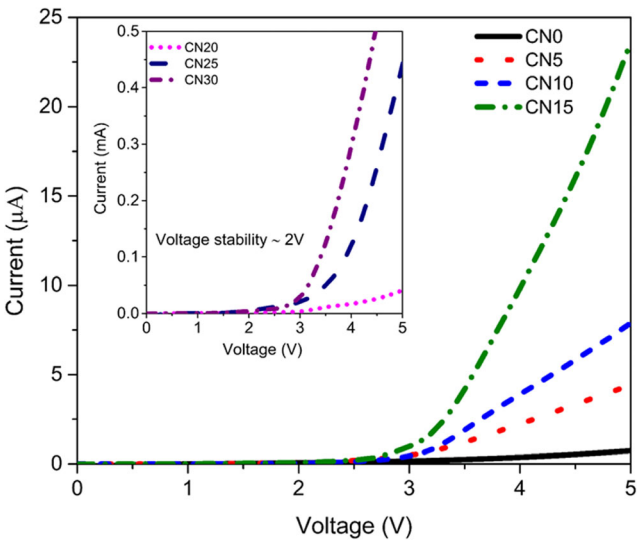

Fig. 10 I-V characteristics of the SPE in the voltage range 0–5 V

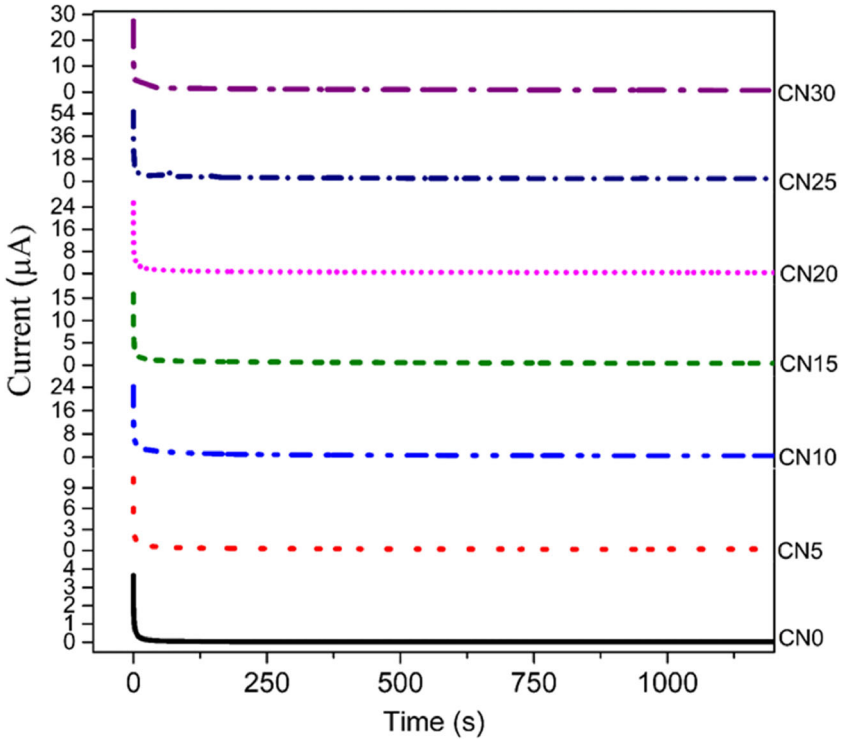

Fig. 11 Transference number measurement for SPE system

and the band at the higher wavenumber side (1444–1456 cm^{-1}) is assigned to ion pairs $Na^{+}\cdots NO_3^{-}$ [28, 29, 62, 63].

Percentage of free ions in the NaCMC:$NaNO_3$ SPE was evaluated by considering the area under the deconvoluted peak using Eq. (5) [38]

$$Percentage\ of\ free\ ion(\%) = \frac{A_f}{A_f + A_c} \times 100\% \tag{5}$$

where A_f represents the area under the peak corresponding to free ions and A_c represents the area under the peak corresponding to ion-aggregates (contact ions). The transport parameter such as the number of mobile ions (η), ionic mobility (μ) and diffusion coefficient (D) was calculated by Eqs. (6), (7), (8) and (9).

$$\eta = \frac{MN_A}{V_{Total}} \times free\ ion\ (\%) \tag{6}$$

$$V_{Total} = \left[\frac{weight}{density}(NaCMC)\right] + \left[\frac{weight}{density}(NaNO_3)\right] \tag{7}$$

$$\mu = \frac{\sigma}{\eta e} \tag{8}$$

$$D = \frac{k_B T \mu}{e} \tag{9}$$

where M is the number of moles of dopant ($NaNO_3$), N_A is the Avogadro's constant (6.02×10^{23}/mol), V_{Total} is the total volume of SPEs system, k_B is the Boltzmann constant (1.38×10^{23} JK^{-1}), T is the absolute temperature in Kelvin and e is the electric charge (1.602×10^{-19}C).

From Table 5, it could be observed that the percentage of free ions has steadily increased up to CN25, due to complete dissociation of salt into free ions. However, for CN30 the percentage of free ion has reduced due to the association of

Table 6 Mechanical properties of NaCMC and $NaNO_3$ doped NaCMC films

Sample	Tensile strength (MPa)	Elongation at break (%)	Youngs modulus (MPa)
CN0	55.00	3.02	1912.07
CN5	49.34	9.16	1949.49
CN10	45.97	17.15	1464.60
CN15	42.03	35.98	1009.71
CN20	35.25	29.66	805.18
CN25	37.62	33.14	741.61
CN30	30.12	30.64	643.03

ions leading to salt aggregation, well supported by FTIR that exhibits a peak of NO_3^- at 832 cm^{-1} implying that availability of functional group is not sufficient to dissociate the salt and thus leading to ion aggregates [64]. Even though the percentage of free ions is low for the highest conducting SPE, ionic conductivity is strongly associated with mobility and diffusion coefficient [65].

σ_{dc} and ε' follow the same trend with an increase in salt concentration for samples CN5-CN25, indicating that $\sigma_{dc} \propto n \propto \varepsilon'$ and directing on the fact that enhancement in conductivity is due to an increase in charge carrier concentration, also observed from FTIR deconvolution technique. A considerable variation in conductivity and relaxation time for CN30 sample is primarily due to an increase in ion mobility as observed in Table 5, as it is highly amorphous. Further doping has not been carried out, due to formation of ion aggregates as noticed from FTIR spectra.

I-V characteristics and transference number

The voltage stability of the films was analyzed by measuring the variation of residual electronic current as the function of the applied voltage, as depicted in Fig. 10. An abrupt hike in the current is observed at ~ 2V for all the samples, indicating its voltage stability window [66]. Transference number informs about the contribution of a specific charged particle to the total conductivity. DC biasing of SPE, sandwiched between the stainless-steel electrode below the decomposition potential was performed. DC biasing leads to the migration of ions towards opposite electrodes until the steady-state condition is reached, i.e. SS/SPE/SS; the cell is completely polarized, and thereafter, residual electronic current flows because of the migration across the electrolyte interface. Initial current before polarization were contributed by both ions and electron that falls rapidly with time, whereas the steady current is reached solely due to electrons. The polarization current as the function of time is monitored in DC Voltage bias of 1.5 V across the SS/electrolyte/SS cell as depicted in Fig. 11. The total ionic transference number is calculated using the relation $t_{ion} = \frac{I_i - I_s}{I_i}$, where I_i, initial current at time $t = 0$ and I_s , steady-state current/residual electronic current [67]. Ionic transference number obtained for SPEs are found to be in the range 0.97–0.99, ensuring that the conductivity is mainly due to ions and electronic contribution to the total current is negligible.

Mechanical properties

In addition to ionic conductivity, the mechanical property of the SPE, such as elastic modulus, plays a vital role in the battery performance [68], and hence it is necessary to develop SPE with high ionic conductivity and sufficient mechanical strength at the operating temperature**.** Mechanical properties, Young's modulus, elongation at break and tensile strength

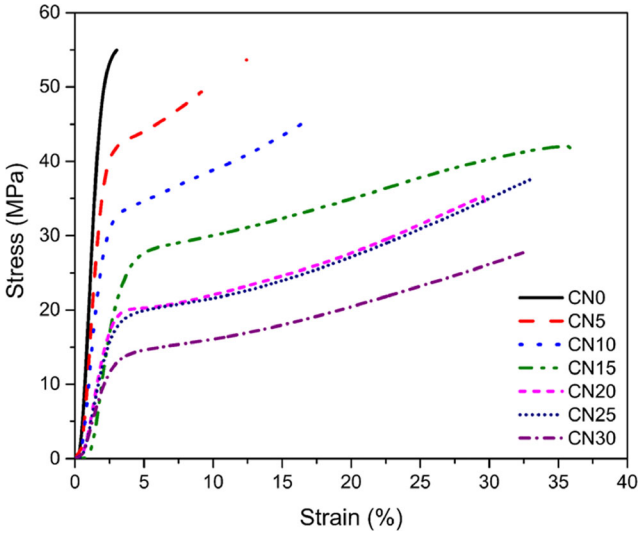

Fig. 12 Stress-strain curve of NaCMC and $NaNO_3$ doped NaCMC films

were quantitatively analyzed by a stress-strain curve for SPEs, shown in Fig. 12 and are tabulated in Table 6. The pristine is brittle, since it has an elongation at break < 5%, and the softness as well as the flexibility of SPEs change with an increase in salt concentration and turn out to be an elastomer [69]. The mechanical properties of the SPE should have been deteriorated with increases in salt concentration, as the weight percentage of NaCMC has decreased. However, anomalous behaviour has been observed in the mechanical properties of the films with increase in salt concentration. As observed in FTIR spectraas well as in the DSC curve, the enhancement in the mechanical properties that have been observed for a certain weight percentage of salt in the matrix maybe due to increase in the hydrogen bonding between the anion and functional group of the polymer [70]. Yue at al. [71] reported the minimum requirement for all-solid-state polymer electrolytes in LIBs with mechanical property to be ≥30 MPa. The highest conducting SPE (CN30) has sufficient mechanical strength to be incorporated in an electrochemical cell.

Conclusion

A new solid biopolymer electrolyte system based on NaCMC doped with sodium nitrate was prepared by solution casting technique. FTIR and XRD analysis of the films confirmed that NaCMC polymer has salt-solvating power, and the microstructural modification that was observed in the electrolyte system upon doping was due to the formation of hydrogen bonding between the oxygen of NO_3^- ion with the hydrogen atom of the functional group attached to the main chain of NaCMC. An increase in T_g upon addition of $NaNO_3$ was due to the stiffening of polymer chains owing to anion-polymer interaction. The frequency-dependent electrical study showed an enhancement in the dielectric permittivity and

ionic conductivity with an increase in salt content, which was due to an increase in charge carrier concentration and not because of segmental motion of polymer chains as confirmed from the DSC study, thus exhibiting a one-to-one correlation between the dielectric constant, carrier concentration and ionic conductivity. The transference number obtained for the SPEs confirms that ions are predominant carriers. An increase in conductivity upon doping was not only because of increment in charge carrier concentration but also due to an increase amorphousness and thus leading to an increase in ion-mobility as confirmed through the FTIR deconvolution technique. NaCMC doped with 30 wt% of $NaNO_3$ showed exceptionally high ionic conductivity of 3×10^{-3} Scm^{-1} compared with other doped films with low crystallinity, confirming it to be a more amorphous film, with the ultimate mechanical strength of 30.12 MPa.

Funding Open access funding provided by Manipal Academy of Higher Education, Manipal. The authors are thankful to UGC DAE Consortium for Scientific Research (Kolkata Centre), Government of India, for financial assistance in the form of Research Project (Sanction No. UGC-DAE-CSR-KC/CRS/19/MS010/0931/0971 dated 10-05-2019).

Declarations

Conflict of interest The authors declare no competing interests.

References

1. Kubota K, Dahbi M, Hosaka T, Kumakura S, Komaba S (2018) Towards K-Ion and Na-Ion batteries as 'beyond Li-Ion. Chem Rec 18(4):459–479. https://doi.org/10.1002/tcr.201700057
2. Yabuuchi N, Kubota K, Dahbi M, Komaba S (2014) Research development on sodium-ion batteries. Chem Rev 114(23):11636–11682. https://doi.org/10.1021/cr500192f
3. Hwang J-Y, Myung S-T, Sun Y-K (2017) Sodium-ion batteries: present and future. Chem Soc Rev 46(12):3529–3614. https://doi.org/10.1039/C6CS00776G
4. Ponrouch A, Monti D, Boschin A, Steen B, Johansson P, Palacín MR (2015) Non-aqueous electrolytes for sodium-ion batteries. J Mater Chem A 3(1):22–42. https://doi.org/10.1039/C4TA04428B
5. Winie T, Arof AK, Thomas S (2019) Polymer electrolytes: characterization techniques and energy applications. John Wiley & Sons, Hoboken
6. Wright PV (2002) Developments in polymer electrolytes for lithium batteries. MRS Bull 27(8):597–602. https://doi.org/10.1557/mrs2002.194
7. Pradhan DK, Karan NK, Thomas R, Katiyar RS (2014) Coupling of conductivity to the relaxation process in polymer electrolytes. Mater Chem Phys 147(3):1016–1021. https://doi.org/10.1016/j.matchemphys.2014.06.053
8. Zhou D, Shanmukaraj D, Tkacheva A, Armand M, Wang G (2019) Polymer electrolytes for lithium-based batteries: advances and prospects. Chem 5(9):2326–2352. https://doi.org/10.1016/j.chempr.2019.05.009
9. Agrawal RC, Pandey GP (2008) Solid polymer electrolytes: materials designing and all-solid-state battery applications: an overview. J Phys D Appl Phys 41(22):223001. https://doi.org/10.1088/0022-3727/41/22/223001
10. Singh KP, Gupta PN (1998) Study of dielectric relaxation in polymer electrolytes. Eur Polym J 34(7):1023–1029. https://doi.org/10.1016/S0014-3057(97)00207-3
11. Aziz SB, Woo TJ, Kadir MFZ, Ahmed HM (2018) A conceptual review on polymer electrolytes and ion transport models. J Sci Adv Mater Device 3(1):1–17. https://doi.org/10.1016/j.jsamd.2018.01.002
12. Samsudin AS, Khairul WM, Isa MIN (2012) Characterization on the potential of carboxy methylcellulose for application as proton conducting biopolymer electrolytes. J Non-Cryst Solids 358(8):1104–1112. https://doi.org/10.1016/j.jnoncrysol.2012.02.004
13. Almasi H, Ghanbarzadeh B, Entezami AA (2010) Physicochemical properties of starch–CMC–nanoclay biodegradable films. Int J Biol Macromol 46(1):1–5. https://doi.org/10.1016/j.ijbiomac.2009.10.001
14. Feddersen RL, Thorp SN (1993) CHAPTER 20 - Sodium Carboxymethylcellulose. In: Whistler RL, Bemiller JN (eds) Industrial Gums, Third edn. Academic Press, London, pp 537–578
15. Chen Z, Kim GT, Chao D, Loeffler N, Copley M, Lin J, Shen Z, Passerini S (Dec. 2017) Toward greener lithium-ion batteries: aqueous binder-based LiNi0.4Co0.2Mn0.4O2 cathode material with superior electrochemical performance. J Power Sources 372:180–187. https://doi.org/10.1016/j.jpowsour.2017.10.074
16. Zhao T, Meng Y, Ji R, Wu F, Li L, Chen R (2019) Maintaining structure and voltage stability of Li-rich cathode materials by green water-soluble binders containing Na+ ions. J Alloys Compd 811:152060. https://doi.org/10.1016/j.jallcom.2019.152060
17. Gupta S, Varshney PK (2019) Effect of plasticizer on the conductivity of carboxymethyl cellulose-based solid polymer electrolyte. In: Polym. Bull. https://doi.org/10.1007/s00289-019-02714-1
18. Ahmad NH, Isa MIN (2016) Characterization of un-plasticized and propylene carbonate plasticized carboxymethyl cellulose doped ammonium chloride solid biopolymer electrolytes. Carbohydr Polym 137:426–432. https://doi.org/10.1016/j.carbpol.2015.10.092
19. Samsudin AS, Khairul WM, Isa MIN (2012) Characterization on the potential of carboxy methylcellulose for application as proton conducting biopolymer electrolytes. J Non-Cryst Solids 358(8):1104–1112. https://doi.org/10.1016/j.jnoncrysol.2012.02.004
20. Chai MN, Isa MIN (2016) Novel proton conducting solid biopolymer electrolytes based on carboxymethyl cellulose doped with oleic acid and plasticized with glycerol. Sci Rep 6. https://doi.org/10.1038/srep27328
21. Rivas BL, Pereira ED, Moreno-Villoslada I (2003) Water-soluble polymer–metal ion interactions. Prog Polym Sci 28(2):173–208. https://doi.org/10.1016/S0079-6700(02)00028-X
22. Pushpamalar V, Langford SJ, Ahmad M, Lim YY (2006) Optimization of reaction conditions for preparing carboxymethyl

cellulose from sago waste. Carbohydr Polym 64(2):312–318. https://doi.org/10.1016/j.carbpol.2005.12.003
23. Teoh KH, Ramesh S, Arof AK (2012) Investigation on the effect of nanosilica towards corn starch–lithium perchlorate-based polymer electrolytes. J Solid State Electrochem 16(10):3165–3170. https://doi.org/10.1007/s10008-012-1741-4
24. Biswal DR, Singh RP (2004) Characterisation of carboxymethyl cellulose and polyacrylamide graft copolymer. Carbohydr Polym 57(4):379–387. https://doi.org/10.1016/j.carbpol.2004.04.020
25. Samsudin AS, Saadiah MA (2018) Ionic conduction study of enhanced amorphous solid bio-polymer electrolytes based carboxymethyl cellulose doped NH4Br. J Non-Cryst Solids 497:19–29. https://doi.org/10.1016/j.jnoncrysol.2018.05.027
26. Rajeh A, Morsi MA, Elashmawi IS (2019) Enhancement of spectroscopic, thermal, electrical and morphological properties of polyethylene oxide/carboxymethyl cellulose blends: Combined FT-IR/DFT. Vacuum 159:430–440. https://doi.org/10.1016/j.vacuum.2018.10.066
27. Ren Z, Xu X, Wang X, Gao B, Yue Q, Song W, Zhang L, Wang H (2016) FTIR, Raman, and XPS analysis during phosphate, nitrate and Cr (VI) removal by amine cross-linking biosorbent. J Colloid Interface Sci 468:313–323. https://doi.org/10.1016/j.jcis.2016.01.079
28. Bourahla S, Ali Benamara A, Kouadri Moustefai S (2013) Infrared spectra of inorganic aerosols: ab initio study of (NH4)2SO4, NH4NO3, and NaNO3. Can J Phys 92(3):216–221. https://doi.org/10.1139/cjp-2013-0367
29. Ehrhardt C, Gjikaj M, Brockner W (2005) Thermal decomposition of cobalt nitrato compounds: preparation of anhydrous cobalt (II) nitrate and its characterisation by Infrared and Raman spectra. Thermochim Acta 432(1):36–40. https://doi.org/10.1016/j.tca.2005.04.010
30. Anantha PS, Hariharan K (2005) Physical and ionic transport studies on poly (ethylene oxide)–NaNO3 polymer electrolyte system. Solid State Ionics 176(1):155–162. https://doi.org/10.1016/j.ssi.2004.07.006
31. Shukur MF, Kadir MFZ (2015) Electrical and transport properties of NH4Br-doped cornstarch-based solid biopolymer electrolyte. Ionics 21(1):111–124. https://doi.org/10.1007/s11581-014-1157-5
32. "Infrared spectroscopy: fundamentals and applications | Wiley," Wiley.com. https://www.wiley.com/ens/Infrared+Spectroscopy%3A+Fundamentals+and+Applications-p-9780470854280 ().
33. de Melo EM, Clark JH, Matharu AS (2017) The Hy-MASS concept: hydrothermal microwave assisted selective scissoring of cellulose for in situ production of (meso) porous nanocellulose fibrils and crystals. Green Chem 19(14):3408–3417. https://doi.org/10.1039/C7GC01378G
34. Wojdyr M (2010) Fityk: a general-purpose peak fitting program. J Appl Crystallogr 43(5–1):1126–1128. https://doi.org/10.1107/S0021889810030499
35. Sampathkumar L, Christopher Selvin P, Selvasekarapandian S, Perumal P, Chitra R, Muthukrishnan M (2019) Synthesis and characterization of biopolymer electrolyte based on tamarind seed polysaccharide, lithium perchlorate and ethylene carbonate for electrochemical applications. Ionics 25(3):1067–1082. https://doi.org/10.1007/s11581-019-02857-1
36. Ravi M, Pavani Y, Kiran Kumar K, Bhavani S, Sharma AK, Narasimha Rao VVR (2011) Studies on electrical and dielectric properties of PVP:$KBrO_4$ complexed polymer electrolyte films. Mater Chem Phys 130(1):442–448. https://doi.org/10.1016/j.matchemphys.2011.07.006
37. He R, Kyu T (2016) Effect of plasticization on ionic conductivity enhancement in relation to glass transition temperature of crosslinked polymer electrolyte membranes. Macromolecules 49(15):5637–5648. https://doi.org/10.1021/acs.macromol.6b00918
38. Arof AK, Amirudin S, Yusof SZ, Noor IM (2014) A method based on impedance spectroscopy to determine transport properties of polymer electrolytes. Phys Chem Chem Phys 16(5):1856–1867. https://doi.org/10.1039/C3CP53830C
39. Benedict TJ, Banumathi S, Veluchamy A, Gangadharan R, Ahamad AZ, Rajendran S (1998) Characterization of plasticized solid polymer electrolyte by XRD and AC impedance methods. J Power Sources 75(1):171–174. https://doi.org/10.1016/S0378-7753(98)00063-9
40. Ibrahim S, Yasin SMM, Ng MN, Ahmad R, Johan MR (2011) Impedance spectroscopy of carbon nanotube/solid polymer electrolyte composites. Solid State Commun 151(23):1828–1832. https://doi.org/10.1016/j.ssc.2011.08.015
41. Lvovich VF (2012) Impedance spectroscopy: applications to electrochemical and dielectric phenomena. John Wiley & Sons, Hoboken
42. Ramesh S, Arof AK (2001) Ionic conductivity studies of plasticized poly (vinyl chloride) polymer electrolytes. Mater Sci Eng B 85(1):11–15. https://doi.org/10.1016/S0921-5107(01)00555-4
43. Winie T, Arof AK, Thomas S (2019) Polymer electrolytes: characterization techniques and energy applications. Wiley, Hoboken
44. Arya A, Sadiq M, Sharma AL (2019) Salt concentration and temperature dependent dielectric properties of blend solid polymer electrolyte complexed with NaPF6. Mater Today: Proc 12:554–564. https://doi.org/10.1016/j.matpr.2019.03.098
45. Pal P, Ghosh A (2018) Investigation of ionic conductivity and relaxation in plasticized PMMA-LiClO4 solid polymer electrolytes. Solid State Ionics 319:117–124. https://doi.org/10.1016/j.ssi.2018.02.009
46. Ishai PB, Talary MS, Caduff A, Levy E, Feldman Y (2013) Electrode polarization in dielectric measurements: a review. Meas Sci Technol 24(10):102001. https://doi.org/10.1088/0957-0233/24/10/102001
47. Funke K (1993) Jump relaxation in solid electrolytes. Prog Solid State Chem 22(2):111–195. https://doi.org/10.1016/0079-6786(93)90002-9
48. Funke K (1997) Ion transport in fast ion conductors — spectra and models. Solid State Ionics 94(1):27–33. https://doi.org/10.1016/S0167-2738(96)00500-0
49. Patel HK, Martin SW (1992) Fast ionic conduction in Na 2 S+ B 2 S 3 glasses: compositional contributions to nonexponentiality in conductivity relaxation in the extreme low-alkali-metal limit. Phys Rev B 45(18):10292
50. Ratner MA, Shriver DF (1988) Ion transport in solvent-free polymers. Chem Rev 88(1):109–124. https://doi.org/10.1021/cr00083a006
51. Raymond C, Ronca S (2017) Chapter 6 - Relation of structure to electrical and optical properties. In: Gilbert M (ed) Brydson's Plastics Materials, Eighth edn. Butterworth-Heinemann, Oxford, pp 103–125
52. A. J. Stamm, "Wood and cellulose science.," Wood and cellulose science., 1964, . [Online]. Available: https://www.cabdirect.org/cabdirect/abstract/19640604227.
53. Majid SR, Arof AK (2007) Electrical behavior of proton-conducting chitosan-phosphoric acid-based electrolytes. Phys B Condens Matter 390(1):209–215. https://doi.org/10.1016/j.physb.2006.08.038
54. Dam T, Tripathy SN, Paluch M, Jena SS, Pradhan DK (2016) Investigations of relaxation dynamics and observation of nearly constant loss phenomena in PEO20-LiCF3SO3-ZrO2 based polymer nano-composite electrolyte. Electrochim Acta 202:147–156. https://doi.org/10.1016/j.electacta.2016.03.134
55. El Shafee E (1996) Dielectric and conductivity relaxation in sodium carboxymethyl cellulose and its acid form. Carbohydr Polym 31(1):93–98. https://doi.org/10.1016/S0144-8617(96)00053-7

56. Agrawal SL, Awadhia A (2004) DSC and conductivity studies on PVA based proton conducting gel electrolytes. Bull Mater Sci 27(6):523–527. https://doi.org/10.1007/BF02707280
57. Ramya CS, Selvasekarapandian S, Hirankumar G, Savitha T, Angelo PC (2008) Investigation on dielectric relaxations of PVP–NH4SCN polymer electrolyte. J Non-Cryst Solids 354(14):1494–1502. https://doi.org/10.1016/j.jnoncrysol.2007.08.038
58. Arya A, Sharma AL (2018) Effect of salt concentration on dielectric properties of Li-ion conducting blend polymer electrolytes. J Mater Sci Mater Electron 29(20):17903–17920. https://doi.org/10.1007/s10854-018-9905-3
59. Bhargav PB, Mohan VM, Sharma A, Rao VN (2009) Investigations on electrical properties of (PVA: NaF) polymer electrolytes for electrochemical cell applications. Curr Appl Phys 9(1):165–171. https://doi.org/10.1016/j.cap.2008.01.006
60. Pradhan DK, Choudhary RNP, Samantaray BK (2008) Studies of dielectric relaxation and ac conductivity behavior of plasticized polymer nanocomposite electrolytes. Int J Electrochem Sci 3:12–561. https://doi.org/10.1016/j.matchemphys.2009.01.008
61. Saadiah MA, Zhang D, Nagao Y, Muzakir SK, Samsudin AS (May 2019) Reducing crystallinity on thin film based CMC/PVA hybrid polymer for application as a host in polymer electrolytes. J Non-Cryst Solids 511:201–211. https://doi.org/10.1016/j.jnoncrysol.2018.11.032
62. Papke BL, Ratner MA, Shriver DF (1982) Vibrational spectroscopic determination of structure and ion pairing in complexes of poly (ethylene oxide) with lithium salts. J Electrochem Soc 129(7):1434. https://doi.org/10.1149/1.2124179
63. Pritam AA, Sharma AL (2019) Dielectric relaxations and transport properties parameter analysis of novel blended solid polymer electrolyte for sodium-ion rechargeable batteries. J Mater Sci 54(9):7131–7155. https://doi.org/10.1007/s10853-019-03381-3
64. Sångeland C, Mogensen R, Brandell D, Mindemark J (2019) Stable cycling of sodium metal all-solid-state batteries with polycarbonate-based polymer electrolytes. ACS Appl Polym Mater 1(4):825–832. https://doi.org/10.1021/acsapm.9b00068
65. Mazuki NF, Fuzlin AF, Saadiah MA, Samsudin AS (2019) An investigation on the abnormal trend of the conductivity properties of CMC/PVA-doped NH4Cl-based solid biopolymer electrolyte system. Ionics 25(6):2657–2667. https://doi.org/10.1007/s11581-018-2734-9
66. Sharma AL, Thakur AK (2010) Improvement in voltage, thermal, mechanical stability and ion transport properties in polymer-clay nanocomposites. J Appl Polym Sci 118(5):2743–2753. https://doi.org/10.1002/app.32677
67. Bhargav PB, Mohan VM, Sharma AK, Rao VVRN (2009) Investigations on electrical properties of (PVA:NaF) polymer electrolytes for electrochemical cell applications. Curr Appl Phys 9(1):165–171. https://doi.org/10.1016/j.cap.2008.01.006
68. Sakuda A, Hayashi A, Tatsumisago M (2013) Sulfide Solid Electrolyte with Favorable Mechanical Property for All-Solid-State Lithium Battery. Sci Rep 3(1):1. https://doi.org/10.1038/srep02261
69. Landel RF, Nielsen LE (1993) Mechanical properties of polymers and composites. CRC Press, Boca Raton
70. Xiao C, Lu Y, Liu H, Zhang L (2001) Preparation and characterization of konjac glucomannan and sodium carboxymethylcellulose blend films. J Appl Polym Sci 80(1):26–31. https://doi.org/10.1002/1097-4628(20010404)80:1<26::AID-APP1070>3.0.CO;2-B
71. Yue L, Ma J, Zhang J, Zhao J, Dong S, Liu Z, Cui G, Chen L (2016) All solid-state polymer electrolytes for high-performance lithium ion batteries. Energy Storage Mater 5:139–164. https://doi.org/10.1016/j.ensm.2016.07.003